

## ON THE ABSORPTION OF X-RAYS IN THE INTERSTELLAR MEDIUM

J. WILMS

Institut für Astronomie und Astrophysik, Abt. Astronomie  
Waldhäuser Straße 64, D-72076 Tübingen, Germany

AND

A. ALLEN, R. MCCRAY

JILA, University of Colorado  
Campus Box 440, Boulder, CO 80309-0440, USA

*Astrophysical Journal, in press*

### ABSTRACT

We present an improved model for the absorption of X-rays in the interstellar medium (ISM) intended for use with data from future X-ray missions with larger effective areas and increased energy resolution such as *Chandra* and the X-ray Multiple Mirror mission, in the energy range  $\gtrsim 100$  eV. Compared to previous work, our formalism includes recent updates to the photoionization cross section and revised abundances of the interstellar medium, as well as a treatment of interstellar grains and the H<sub>2</sub> molecule. We review the theoretical and observational motivations behind these updates and provide a subroutine for the X-ray spectral analysis program XSPEC that incorporates our model.

*Subject headings:* Atomic data — ISM: abundances — dust, extinction — X-rays: ISM

### 1. INTRODUCTION

The precise knowledge of the modification of X-ray radiation in the interstellar medium (ISM) is of crucial importance for the understanding of X-ray spectra from cosmic sources since the observed X-ray spectra have to be corrected for this modification before interpreting the observed data. The current state of the art in the computation of the energy-dependent photoionization cross section of the ISM,  $\sigma_{\text{ISM}}$ , has been summarized by Bałucińska-Church & McCammon (1992, BM92). These authors greatly improved<sup>1</sup> the precision in the computation of  $\sigma_{\text{ISM}}$  compared to previous implementations (Strom & Strom 1961; Brown & Gould 1970; Fireman 1974; Ride & Walker 1977; Morrison & McCammon 1983, MM83) by allowing to adjust the assumed abundances of the ISM and by using polynomial fits to the photoionization cross sections of Henke et al. (1982).

Although the BM92 model provides sufficient precision for the data analysis with current instruments, the advent of X-ray missions with instruments of high energy resolution and large effective areas, such as *Chandra* or the Newton X-ray Multiple Mirror mission (XMM-Newton), will result in large improvements in the precision of X-ray astronomical measurements. It is therefore necessary to have tools at hand that reflect the current understanding of the physics of the interaction of X-rays with the ISM at the percent level.

In this paper we improve on the models of BM92 by incorporating recent improvements in the photoionization cross sections and by taking into account the physics of the interstellar dust and the molecular phase of the interstellar medium. Section 2 describes the formalism employed to compute  $\sigma_{\text{ISM}}$ . We describe the atomic physics data (§2.2)

and explain our choices of elemental and molecular abundances (§2.3) as well as dust grain parameters (§2.4). We summarize the model, compare it to previous models, and point out its remaining shortcomings in Section 3. In the appendices, we derive the influence of dust on  $\sigma_{\text{ISM}}$  (Appendix A) and describe the implementation of our model into XSPEC (Appendix B).

The intended readership of this paper consists of users of the new missions, many of whom do not intend to become specialists on the ISM. We have therefore attempted to include sufficient information to make this paper self-contained, and have chosen a review-like style.

### 2. MODELING THE X-RAY ABSORPTION IN THE ISM

#### 2.1. X-ray Absorptivity in the ISM

The total photoionization cross section of the ISM,  $\sigma_{\text{ISM}}$ , is obtained by summing over the contributions of the astrophysically relevant elements. Taking into account the phases of the ISM,  $\sigma_{\text{ISM}}$  can be written as

$$\sigma_{\text{ISM}} = \sigma_{\text{gas}} + \sigma_{\text{molecules}} + \sigma_{\text{grains}}. \quad (1)$$

As is common for X-ray applications, we normalize  $\sigma_{\text{ISM}}$  to the total hydrogen number density (i.e., in molecular, neutral, or ionized form),  $N_{\text{H}}$ , so that the observed X-ray spectrum of a source,  $I_{\text{obs}}$ , is given by

$$I_{\text{obs}}(E) = e^{-\sigma_{\text{ISM}}(E) N_{\text{H}}} I_{\text{source}}(E), \quad (2)$$

where  $N_{\text{H}}$  is measured in atoms cm<sup>-2</sup> and  $I_{\text{source}}(E)$  is the X-ray spectrum as emitted by the X-ray source. We drop the explicit energy dependence of  $\sigma_{\text{ISM}}$  for the rest of the paper.

The contribution of the gaseous, non-molecular cold and warm phases of the ISM to  $\sigma_{\text{ISM}}$  is obtained by summing

<sup>1</sup>When referring to the cross sections of BM92 we use their subroutines as implemented as the `phabs` model in XSPEC, version 10.0z (Arnaud 1996). This implementation contains improvements compared to the original publication. Starting with XSPEC, version 11.0, other cross-sections are used in the computation of this model (see §2.2 below).

the photoionization cross sections of the individual atoms and ions in these phases, weighting their contributions by the abundances. Hence,

$$\sigma_{\text{gas}} = \sum_{Z,i} A_Z \cdot a_{Z,i} \cdot (1 - \beta_{Z,i}) \cdot \sigma_{\text{bf}}(Z, i) \quad (3)$$

where we use the notation pioneered by Ride & Walker (1977), in which  $A_Z = N(Z)/N(\text{H})$  is the abundance in number of element  $Z$  with respect to hydrogen,  $a_{Z,i} = N(Z, i)/N(Z)$  is the fraction of ions of element  $Z$  that are in ionization stage  $i$ , and  $\sigma_{\text{bf}}(Z, i)$  is the total photoionization cross section of element  $Z$  in ionization stage  $i$ . The depletion of the elements into grains is taken into account through the “depletion factor”  $1 - \beta_{Z,i}$ .

For the molecular phase of the ISM, only molecular hydrogen needs to be taken into account due to its large abundance ( $\sim 20\%$  of the hydrogen might be molecular, see §2.3). Therefore,

$$\sigma_{\text{molecules}} = A_{\text{H}_2} \sigma_{\text{bf}}(\text{H}_2). \quad (4)$$

For material in the grain phase of the ISM, several complications arise. Since the X-ray optical depth of a large grain can be much greater than one (see Fig. 3), most of the X-ray absorption will occur on its surface. Consequently, the contribution of material “within” the grain to  $\sigma_{\text{ISM}}$  is small. Thus, the net effect of this shielding is that the presence of grains *reduces* the effective absorptivity of the ISM relative to the absorptivity of a completely gaseous medium. As we show in Appendix A, the total optical depth for grains with a size distribution  $dn_{\text{gr}}(a)/da$  is given by

$$\begin{aligned} \tau_{\text{grains}} &= \sigma_{\text{grains}} N_{\text{H}} \\ &= N_{\text{H}} \xi_{\text{g}} \int_0^{\infty} \frac{dn_{\text{gr}}(a)}{da} \sigma_{\text{geom}} (1 - \exp(-\langle\sigma\rangle\langle N\rangle)) da \end{aligned} \quad (5)$$

In the derivation of equation (5) we assume that the grains are of chemically homogeneous composition with an average photoabsorption cross section  $\langle\sigma\rangle$ , and can be approximated as spheres with radius  $a$  and average column density  $\langle N\rangle$  (measured in atoms  $\text{cm}^{-2}$ ). Since the grains are partly transparent to X-rays, their absorption cross section is smaller than the grain geometrical cross section,  $\sigma_{\text{geom}} = \pi a^2$ . Finally, the number of grains per hydrogen atom along the line of sight is  $\xi_{\text{g}}$ . We discuss the validity of these assumptions in Section 2.4 and give explicit formulae for all parameters of equation (5) in Appendix A.

In the following sections we describe the data used for evaluating Eqs. (1) and (5) in greater detail.

## 2.2. Atomic Physics

Despite decades of effort, the knowledge of elemental photoionization cross sections in the X-ray regime is still uncertain. In many cases, therefore, one has to rely on either theoretical work or interpolation along the isoelectronic sequence to obtain usable cross sections, and then use compilations of experimental data to gauge the precision of these theoretical computations. In what follows we will describe the basis of the photoionization cross sections used here, focusing on the region  $E \gtrsim 100 \text{ eV}$ . The emphasis is on the choice of cross sections that are good for instruments with a resolution comparable to the CCDs on

*Chandra* or XMM-Newton. Therefore, we will not make an attempt to include the resonances that are important close to the absorption edges that might well be important for the grating instruments aboard these satellites.

For the computation of the photoionization cross section of H, we use the fitting formula of Band et al. (1990), which provides a very good approximation of the exact, analytic cross section but is much faster to evaluate. The maximum deviation between the Band et al. (1990) formula and the analytical cross section (e.g., Bethe & Salpeter 1957, eq. 71.7, divided by two) is  $\sim 1.5\%$  at energies below 2 keV.

The cross section for helium is taken from the recent theoretical evaluation of Yan, Sadeghpour & Dalgarno (1998). Autoionization resonances occur at energies less than 0.08 keV, and the four strongest resonances are included here (as in BM92), using values from Oza (1986) and Fernley (1987). For energies between 0.1 keV and 1 keV, the helium cross section is *smaller* by a factor of  $\sim 0.9$  to  $\sim 0.6$  than that assumed in the subroutine used by BM92, which is based on theoretical work of Chen, Cooper & Brion (1991) and on experimental data by Marr & West (1976). The Yan, Sadeghpour & Dalgarno (1998) cross section, however, agrees with other more recent theoretical computations (e.g., those of Verner & Yakovlev 1995) and is in agreement with more recent experimental data (Yan, Sadeghpour & Dalgarno 1998, and references therein). It also has the correct  $E^{-3.5}$  asymptote required from non-relativistic quantum theory (Bethe & Salpeter 1957). For implications of this smaller He cross section on studies of the ISM, see, e.g., Arabadjis & Bregman (1999).

For all other elements we use the photoionization cross sections as originally published by Verner et al. (1993) and later updated by Verner & Yakovlev (1995), and which are used in XSPEC version 11.0. These authors fitted the results from Hartree-Dirac-Slater computations of  $\sigma_{\text{bf}}$  for individual subshells to a semi-empirical fitting formula. The major advantage of this semi-empirical fitting formula over previous fitting formulae (such as, e.g., polynomial fits) is that it requires only a small number of fitting parameters to express  $\sigma_{\text{bf}}$  to high accuracy while preserving the correct asymptotical properties. A comparison between the experimental data and these cross sections is presented by Verner & Yakovlev (1995), who focus on the overall agreement throughout the electromagnetic spectrum. In addition, we compared the total photoionization cross sections computed from the fitting formula with the compilation of data presented by Henke, Gullikson & Davis (1993) for the range from 0.1 keV to 10 keV. Except for energies close to the K- and L-shell edges, our comparisons indicate maximum relative deviations between these cross sections on the order of 5% above 1 keV.

In their determination of  $\sigma_{\text{bf}}$  close to the K- and L-shell edges, Henke, Gullikson & Davis (1993) used a linear interpolation through the resonances to the edge energy. Since this edge energy was obtained from experimental data, it includes the effects of energy shifts in the solid state and thus is not representative of the true edge energy for the gaseous state of the materials. Indeed, the difference in edge energy between the solid and the gaseous state can be up to several 10 eV (see, e.g., Nicolosi, Jannitti & Tondello 1991, for an illustrative experimental exam-

ple). In many cases, Henke, Gullikson & Davis also do not consider the different subshell threshold energies. On the other hand, the Verner & Yakovlev (1995) cross sections are based on quantum-mechanical computations that include the resonances, and the edge energy is unaffected by solid state effects. We have checked the precision of the Verner & Yakovlev edge energies by comparing them with the computations of Gould & Jung (1991) which are more appropriate for our work than the Henke et al. (1982) or Henke, Gullikson & Davis (1993) values since they assume the elements to be in the gas phase. For  $Z > 8$  the edge energies of Verner & Yakovlev (1995) agree on the 10 eV level with those of Gould & Jung (1991). For C, N, and O, the edge energies adopted by Verner & Yakovlev (1995) are between those of Henke, Gullikson & Davis (1993) and Gould & Jung (1991). We therefore decided to adopt the Verner & Yakovlev edge energies for this work. Note, however, that these differences in the edge energy are relevant only for instruments with extremely high resolution and are irrelevant for most other work.

For molecular hydrogen we adopt the cross sections reported by Yan, Sadeghpour & Dalgarno (1998) for energies above 85 eV. These cross sections are claimed to be accurate to about 5% and have the correct  $E^{-3.5}$  asymptotics. Albeit outside of our formal energy range ( $E \gtrsim 100$  eV) we note that the fit formula given by Yan, Sadeghpour & Dalgarno (1998, eq. 18) for energies below 85 eV has significant deviations with respect to the tabulated cross sections of Samson & Haddad (1994), on which the Yan, Sadeghpour & Dalgarno values are based. Furthermore the fit formula is non-continuous at 85 eV. For energies between 30 and 85 eV we find that the cross section can be represented by

$$\sigma_{\text{bf},\text{H}_2}(x) = \sum_{i=0}^5 a_i x^{-i} \quad (6)$$

where  $x = E/15.4$  eV and where  $\sigma_{\text{bf}}$  is given in Mbarn ( $= 10^{-18}$  cm<sup>2</sup>). The fit coefficients  $a_i$  are given in Table B1. The maximum deviation between the fit and the tabulated data is less than 1%. We note that the photoabsorption cross section of H<sub>2</sub> is  $\sim 2.85\sigma_{\text{H}}$  which results in an increase over previous estimates of  $\sigma_{\text{ISM}}$  for regions where molecular hydrogen is an important contributor to the total absorptivity (i.e., below  $\sim 1$  keV). Molecular effects were not included in the earlier models, so essentially these models assumed  $\sigma_{\text{bf},\text{H}_2} = 2\sigma_{\text{bf},\text{H}}$ .

### 2.3. Abundances

Naturally, the assumed elemental abundances are of crucial importance for the computation of  $\sigma_{\text{ISM}}$ . While many measurements of gas-phase abundances have been made, measurement of the total gas-plus-dust abundance of the ISM is very difficult. As a result, solar abundances, i.e., abundances determined from analysis of the solar photosphere or (carbonaceous) meteorites, have generally been used as the reference abundance for the ISM (Anders & Ebihara 1982; Grevesse & Anders 1989; Anders & Grevesse 1989; Shull 1993, and references therein). For reference, we list in Table B2 what we consider to be the best estimates of these ‘‘local’’ ISM abundances. We list the logarithmic

abundances by number, normalized to a hydrogen abundance of  $\log A_{\text{H}} = 12$ , based on the meteoritic abundances of Anders & Grevesse (1989). We updated the abundances of C and N using the results of Grevesse et al. (1991) and Grevesse & Noels (1993), respectively. The solar abundance of iron has been the subject of several discussions in recent years (Raassen & Uylings 1998; Kostik, Shchukina & Rutten 1996; Biémont et al. 1991, and references therein). We adopted  $\log A_{\text{Fe}} = 7.50 \pm 0.05$  as recently determined by Grevesse & Sauval (1999) in a critical reevaluation of the available data on Fe I lines. The uncertainty of the solar abundances in Table B2 is  $\sim 0.06$  dex or smaller with the exception of  $\log A_{\text{Ne}}$  and  $\log A_{\text{Ar}}$ , for which the uncertainty is 0.1 dex.

As more abundance measurements have been made outside our solar system, it has become apparent that the total gas plus dust ISM abundances are actually lower than the solar abundances (Sofia, Cardelli & Savage 1994; Savage & Sembach 1996, and references therein). Studies of the carbon abundance reviewed by Snow & Witt (1995) strongly indicate a subsolar abundance of carbon in the ISM, with a probable value of  $\sim 70\%$  solar. Similar reductions of 20% to 30% with respect to solar abundances are also indicated for the other metals (Snow & Witt 1996; Savage & Sembach 1996). This trend is consistent with new measurements of the gas-phase abundance of O, C, and N obtained with the Goddard High Resolution Spectrograph (GHRS) on the Hubble Space Telescope (Meyer, Jura & Cardelli 1998; Meyer, Cardelli & Sofia 1997; Cardelli et al. 1996).

Possible differences between solar and ISM abundances had been noted already at the time of publication of previous models for  $\sigma_{\text{ISM}}$ , and the previous computations of  $\sigma_{\text{ISM}}$  closely reflect the historical changes in the understanding of these local abundances. Ride & Walker (1977), for instance, used abundances that were greater than solar abundances in order to better represent abundance values in an ISM assumed to be chemically enriched by galactic evolution, and the model of BM92 was specifically designed to allow adjustments to the assumed abundances<sup>2</sup>. Now that a consistent picture of lower ISM abundance seems to have emerged, the cosmic abundance needs to be revised in models of  $\sigma_{\text{ISM}}$ . To that end we adopt default recommended abundances for the ISM. These abundance values are listed in Table B2, and refer to the *total* abundance of the elements in either the gaseous or grain phase of the ISM. For C, N, and O, we use the values of Cardelli et al. (1996), Meyer, Cardelli & Sofia (1997), and Meyer, Jura & Cardelli (1998), respectively, while for all other elements we use the abundances given by Snow & Witt (1996, Mg, Si, S, Ca, Ti, Cr, Fe, Ni), or, where no value was recommended by these authors, we assume an abundance of 70% with respect to our adopted solar abundances.

We are aware that these abundances are still very much uncertain; the uncertainties in the general ISM abundances are still on the order of 0.1 dex or higher and also strongly depend on the line of sight. However, we feel that it has been adequately established that solar abundances are enriched with respect to the ISM, and that for most astronomical work using the ISM abundances in Table B2

<sup>2</sup>The abundances available in XSPEC are those of Anders & Grevesse (1989), Feldman (1992), and Anders & Ebihara (1982); in addition, user-specified abundances are possible. The BM92 model allows the user to vary the abundances with respect to these default abundances.

is preferable. Since one may anticipate the need for further revision of the interstellar abundances, we have also included an option to change these default abundances in the XSPEC implementation of our model (Appendix B), as BM92 did.

Due to the appreciable difference in the X-ray cross sections for molecular and neutral hydrogen (§2.2), it is necessary to include the contribution of molecular hydrogen. About half of the hydrogen in the Galaxy as a whole is molecular; however, it is not uniformly distributed (Shull & Beckwith 1982). Surveys of low galactic latitudes indicate that the ratio between H<sub>2</sub> and H I is strongly dependent on the radial distance from the galactic center (Brinks 1990; Bronfman et al. 1988). UV observations of H<sub>2</sub> absorption lines with *Copernicus* and with the ORFEUS II (orbiting and retrievable far- and extreme ultraviolet spectrometer) echelle spectrograph indicate that about 20 . . . 25% of the hydrogen is in H<sub>2</sub> in the local ISM (Savage et al. 1977; Gringel et al. 2000). These results are very line-of-sight dependent, though, with some lines of sight being completely free of H<sub>2</sub>. Because of these large fluctuations in the H<sub>2</sub>/H I ratio, it is thus difficult to choose a “typical value”. In order to include the effect of molecular hydrogen on  $\sigma_{\text{ISM}}$  we therefore choose to use the value of 20% as the default value. To more accurately account for the opacity of molecular hydrogen, however, we strongly recommend that this ratio be set to that corresponding to the line-of-sight to the source. The abundances of other molecules are much smaller so that their inclusion is only necessary for work along line of sights with very high  $N_{\text{H}}$  and hence not within the scope of this paper.

#### 2.4. Grain Physics

Evidence for the presence of dust grains in the ISM comes from the observed interstellar extinction (Fitzpatrick 1999; Mathis 1990), as well as from the fact that the observed abundances of the elements in the ISM are generally less than the abundances assumed for the ISM (Savage & Sembach 1996). The ratio between the observed and the assumed abundances is called the “depletion”,  $\beta_Z$ , of the elements. It is generally assumed that the depletion indicates the presence of dust in the ISM, especially since the most depleted elements, C, O, and Si, are thought to be good candidates for the formation of solids in the ISM (Sofia, Cardelli & Savage 1994; Snow & Witt 1995; Mathis 1996, and references therein).

We have adopted a simplified grain model which assumes spherical grains in an MRN size distribution (Mathis, Rumpl & Nordsieck 1977),

$$\frac{dn_{\text{gr}}(a)}{da} \propto a^{-3.5}, \quad \text{where } a_{\text{min}} \leq a \leq a_{\text{max}}, \quad (7)$$

where typically grain size ranges from 0.025  $\mu\text{m}$  to 0.25  $\mu\text{m}$  (Draine & Lee 1984). While the grain composition and structure is still a matter of debate (Mathis 1996; Dwek 1997; Smith & Dwek 1998; Wolff, Clayton & Gibson 1998), here, we assume composite (“fluffy”) grains, consisting of vacuum inclusions in solids. Thus, the grain density in our model ( $\rho = 1 \text{ g cm}^{-3}$ ) is less than the  $\rho = 2 \text{ g cm}^{-3}$  used in previous models (Fireman 1974; Ride & Walker 1977, , MM83).

We assume chemically homogeneous grains consisting of silicates, graphites, and oxides. We list the adopted

chemical composition of the grains in Table B2 in terms of the “depletion factor”  $1 - \beta_Z$ , the ratio between the *gas* abundance and the *total* interstellar abundance of the elements. Table B2 is based on the compilation of measurements given by Shull (1993), which is in general agreement with later GHRS measurements (Savage & Sembach 1996). Contrary to Shull, we do not assume N to be depleted into grains as is suggested by the observational evidence (Savage & Sembach 1996; Meyer, Cardelli & Sofia 1997). As recommended by Sofia, Cardelli & Savage (1994), we also assume a larger abundance of Fe in grains than that assumed by Shull (1993). For cobalt the values determined by Mullman et al. (1998) are used.

To illustrate the large uncertainties associated with the grain composition, we also list in Table B2 the depletions used by Ride & Walker (1977) and MM83, the previous works which included grains in the computation of  $\sigma_{\text{ISM}}$ . The depletion factors of Ride & Walker (1977), as shown in Table B2, are based on gas-abundance measurements using *Copernicus* data. Only one of the depletion factors of MM83 is based on observation, that for oxygen (de Boer 1979, 1981); for the rest, MM83 considered elements to be either completely depleted into grains or entirely in gas form. This simplifying assumption represents the maximum effect of grains on the ISM opacity.

We note that grains are included here partly for completeness and partly to indicate how changes to the current ISM grain model might affect observations made with the more recent X-ray observatories, and not as an attempt to model the solid state in the interstellar medium. While a “perfect” grain model meeting all abundance and observational requirements remains elusive, our grain model at least adequately reproduces the observed extinction, emission features, and depletions of the diffuse ISM (Mathis 1996). For more detailed work, the assumption of spherical grains must be modified (Mathis 1990).

### 3. CONCLUSIONS AND SUMMARY

#### 3.1. Results

Using equation (1) and the assumptions described above, we compute  $\sigma_{\text{ISM}}$ . The results are shown in Fig. 1, where we display the X-ray absorptivity as  $\sigma_{\text{ISM}}E^3$  to emphasize deviations from the  $E^{-3}$  proportionality of  $\sigma_{\text{bf}}$ . By reading the plot as a “bar-diagram”, it is easy to estimate the relative importance of the contributors to  $\sigma_{\text{ISM}}$ . For energies above the oxygen K-edge at  $\sim 0.5 \text{ keV}$  (see Tab. B2), the X-ray opacity is dominated by the metals, and H and He are relatively unimportant. Below 1 keV, C, N, O, and Ne are the important absorbers, while above 1 keV, Si, S, and Fe are important.

Also clear from Fig. 1 is that the effect of grains on  $\sigma_{\text{ISM}}$  is small for a standard MRN distribution. The effect of grains is found to be less than previous estimates such as MM83 in part because our grain model consists of lower-density porous grains and in part because we calculate  $\sigma_{\text{grains}}$  for an MRN distribution of grain sizes rather than by choosing an average grain size such as 0.3  $\mu\text{m}$  as used by Fireman and others. Thus the greatest number of grains lies in very small grains with  $\tau \ll 1$  above  $\sim 1 \text{ keV}$ , so that self-shielding is not important in these grains. Consequently, for an MRN distribution there are

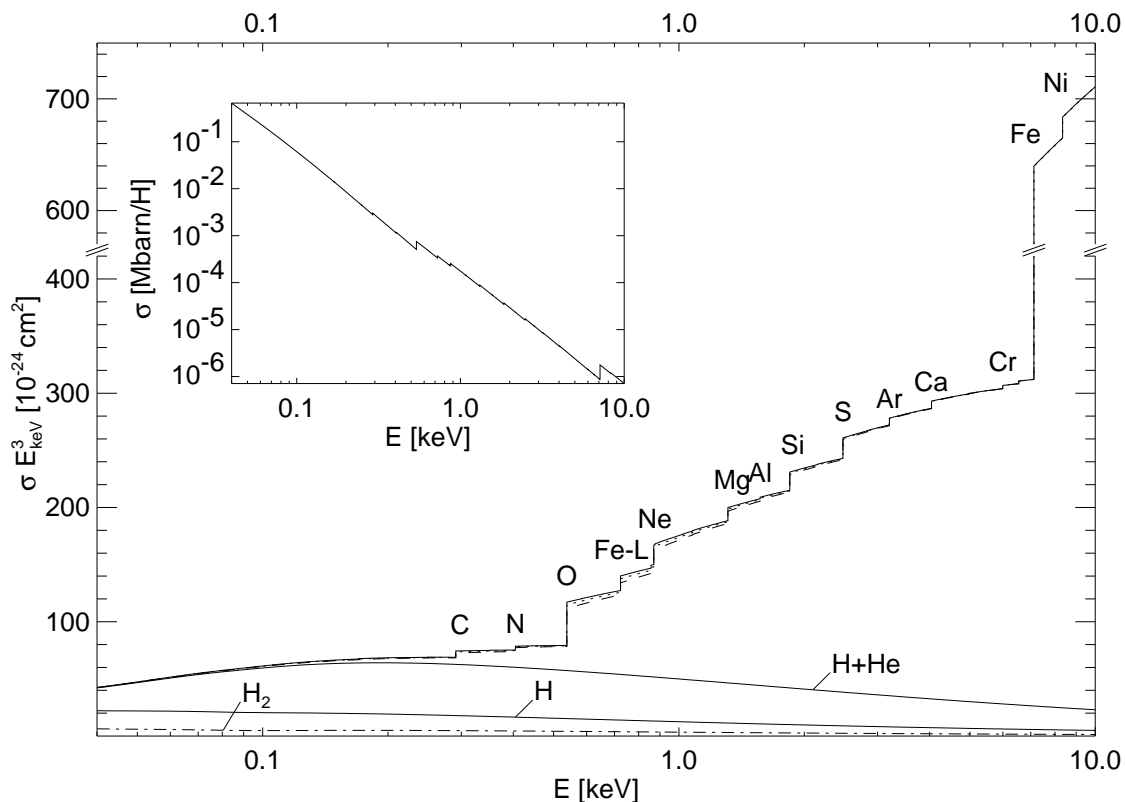


FIG. 1.— Absorptivity per hydrogen atom of the ISM using the assumptions described in the text. The dotted line is the absorptivity including grains with a MRN distribution, and the dashed line is the absorptivity assuming that all grains are of radius  $a = 0.3 \mu\text{m}$ . The inset shows the cross section without the multiplication with  $E^3$ . We also illustrate the contribution of hydrogen and hydrogen plus helium to the total cross section. The contribution of the  $\text{H}_2$  cross section to the total hydrogen cross section is indicated by the dot-dashed line.

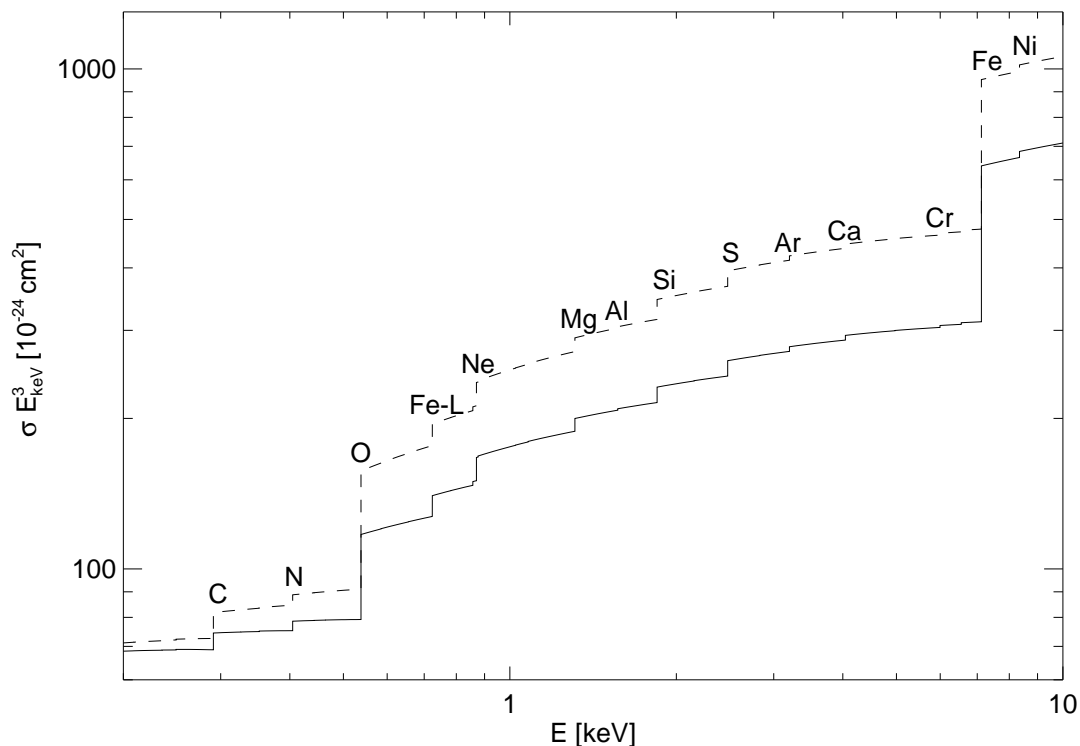


FIG. 2.— Absorptivity per hydrogen atom of the ISM for our adopted ISM abundances (solid line) and for the solar abundances of Tab. B2 (dashed line). For clarity, the cross section has been multiplied with  $E^3$ ; however, the  $y$ -axis is logarithmic here, not linear as in Fig. 1. The revised abundances produce changes in  $\sigma_{\text{ISM}}$  of up to 30% with respect to the solar abundances.

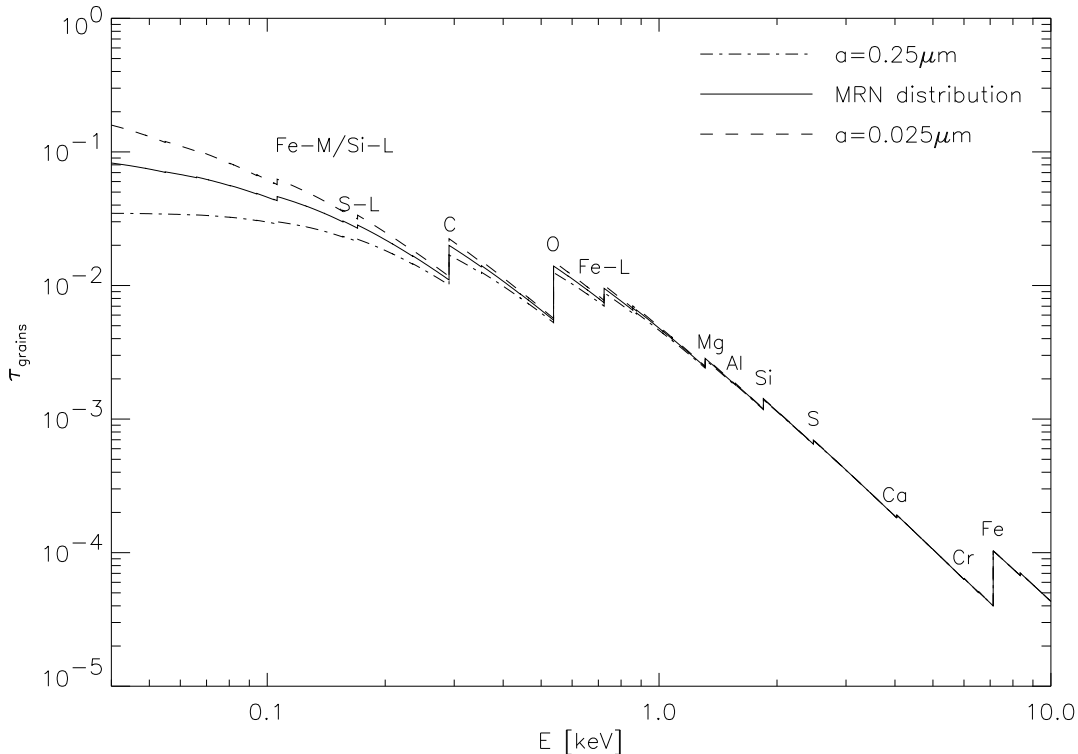


FIG. 3.— Optical depth of grains for a hydrogen column  $N_{\text{H}} = 1.0 \times 10^{20} \text{ cm}^{-2}$  (see Appendix A), and for grains of radius  $a = 0.25 \mu\text{m}$  (dot dashed line) and  $a = 0.025 \mu\text{m}$  (dashed line) as a function of X-ray energy. The total mass in grains is constant. The shielding reduces the optical depth at low energies and for large grain sizes. The labels denote the K-edges of the elements indicated.

only small differences between the optical depth of an entirely gas-phase ISM and the optical depth for an ISM in which some of the gas atoms have been depleted into grains. This is illustrated in Fig. 3, where we plot the grain optical depth as a function of energy for grains of radius  $0.25 \mu\text{m}$  and  $0.025 \mu\text{m}$ , as well as for an MRN distribution of grains. These optical depths are calculated using Appendix A and considering a hydrogen column density  $N_{\text{H}}$  of  $1.0 \times 10^{20} \text{ cm}^{-2}$ . The total mass in grains is the same for all three grain models shown. Clearly, the self-blanketing factor affects the opacity more for low energies and larger grain sizes. Since the change in grain optical depth for the MRN distribution is quite small, grains only slightly modify the absorptivity of the ISM.

We stress, however, that the grain model as used here applies to the diffuse ISM rather than to dense regions such as inner molecular clouds or young stellar objects, where grains might play a much more important role (Mathis 1990). By changing the range of grain sizes from the range adopted here for the diffuse ISM to a grain distribution with larger grains, our formalism (including the XSPEC routine described in Appendix B) can be used to treat these regions as well. As an example, we show in Fig. 1 the influence of grains with  $a = 0.3 \mu\text{m}$ . In this case, X-ray observations will allow the detection of the grains due to the large influence of self-shielding, even with instruments that do not have the high energy resolution to see the solid-state resonance effects close to the absorption edges.

### 3.2. Comparison with previous models

As we outlined in Sect. 2.2 and 2.3, the major differences between this model and the previous models are the updates to the atomic cross sections and the assumed abundances. With the use of simulated observations, we can examine the impact of an updated  $\sigma_{\text{ISM}}$  on the interpretation of observations.

In order to demonstrate the effect of the updates to the cross sections, we compare our values of  $\sigma_{\text{ISM}}$  with those of MM83 and BM92. In Fig. 4a we show the relative deviation between our formulation and that of the earlier models, using our adopted cross-sections and the assumed abundances of the MM83 and BM92 models, respectively. Thus, the figure shows the cumulative effect of the updated cross sections. The differences between the models at photon energies below  $0.3 \text{ keV}$  are mainly a result of the uncertainty in the He cross section. Additional peaks at the K- and L-shell edges are due to  $\sim 10 \text{ eV}$  discrepancies in the assumed edge energy between these models (§2.2) and are not relevant for practical work with moderate resolution instruments. The difference in the values of  $\sigma_{\text{bf}}$  produces the curvature of the relative deviation. The missing subshell absorption edges in the MM83 model are also readily apparent.

In Fig. 4b, we again show the relative deviation between our model and that of the earlier models, but this time using our default *solar* abundance (Table B2) for the abundances in our model, including the additional elements not contained in the MM83 and BM92 models, as well as the  $\text{H}_2$  molecule (important especially below  $\sim 300 \text{ eV}$ ). In this figure, all models are with “solar” abundances, but the dis-

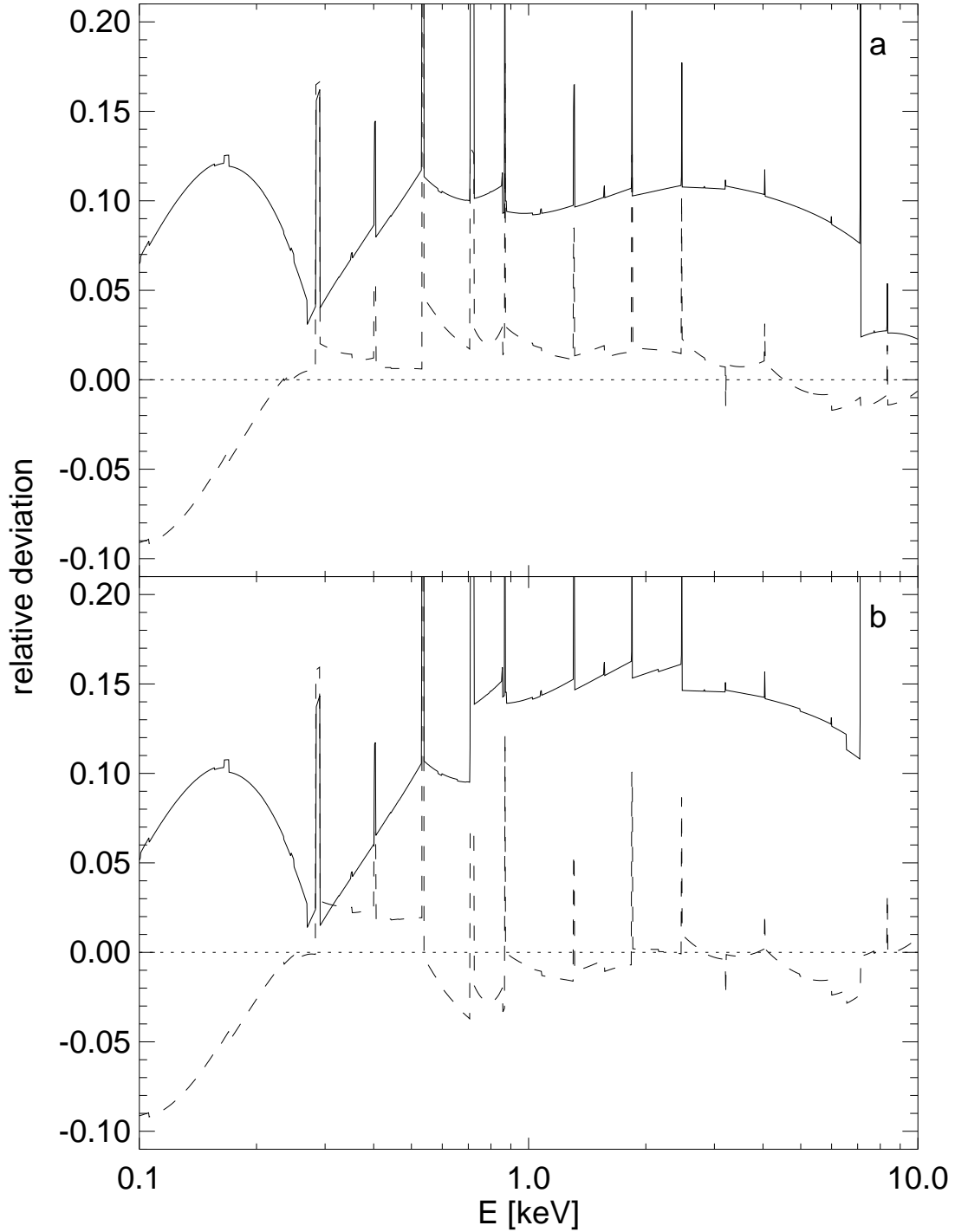


FIG. 4.— Relative deviation of the cross sections of BM92 (solid line) and MM83 (dashed) from the model described here. The relative computation is given as  $(\sigma_i - \sigma)/\sigma$  where  $i = \text{BM92 or MM83}$ , and where  $\sigma$  is our formulation. The spikes at the K- and L-absorption edges are due to slight differences in the assumed edge energies. a: Relative deviation computed using the abundances of BM92 and MM83, respectively. This figure highlights the effect of the change in the cross-sections. b: Relative deviation to our model, computed using the solar abundances of Tab. B2, illustrating the cumulative effect of using different default solar abundances and changing cross sections. See §2.2 for further discussion.

agreement between the “solar” abundances used by the different authors results in 10% of the difference between the three models compared in Fig. 4. However, the difference resulting from different values of the “solar” abundance is small compared to the difference that results from using our default abundance values which are reduced with respect to solar abundances. The discrepancy in  $\sigma_{\text{ISM}}$  which results from the use of our default ISM abundances instead of the solar abundances indicated in Table B2 is shown in Fig. 2.

In order to illustrate the observable changes introduced by our updated model of  $\sigma_{\text{ISM}}$ , we studied these effects using simulations of observations. We simulated the observation of a bright X-ray source which has a pure power-law spectrum with photon index  $\Gamma = -1.7$ , and a normalization of  $A_{\text{PL}} = 2 \text{ ph cm}^{-2} \text{ s}^{-1} \text{ keV}^{-1}$  at 1 keV. Such a source spectrum is characteristic, e.g., of Cygnus X-1 in the hard state (Dove et al. 1998). We then used two values of hydrogen column,  $N_{\text{H}} = 6 \times 10^{21} \text{ cm}^{-2}$  and  $N_{\text{H}} = 6 \times 10^{22} \text{ cm}^{-2}$ , to produce the absorbed spectrum using our model for  $\sigma_{\text{ISM}}$ , using our assumed interstellar abundances. The two values for  $N_{\text{H}}$  are necessary to illustrate the effects of  $N_{\text{H}}$  both in the low energy band (small  $N_{\text{H}}$ ) and in the high energy band (large  $N_{\text{H}}$ ). We simulated an observation by folding the photon spectrum through the detector response matrix and adding Poisson noise. To ensure comparable signal-to-noise ratios in all simulated observations, the exposure times were chosen such that  $10^6$  photons were contained in the resulting spectrum. The detectors we chose to represent current instruments were SIS on the Advanced Satellite for Cosmology and Astronomy (ASCA) for the low  $N_{\text{H}}$  simulation, and the Proportional Counter Array (PCA) on the Rossi X-ray Timing Explorer (RXTE) for the large  $N_{\text{H}}$  simulation. The detector chosen to represent the quality and energy resolution of the future missions is the European Photon Imaging Camera (EPIC) pn CCD on XMM-Newton. In neither case did we take photon pileup or other instrumental effects such as a saturation of the telemetry bandwidth into account.

The resulting simulated photon spectrum was rebinned and analyzed using the MM83 and the BM92 models for  $\sigma_{\text{ISM}}$ . In Fig. 5 we present the ratio between the data and the resulting best-fit model using the MM83 model (the BM92 model without varying the abundances gave qualitatively the same results). For the PCA and the SIS, the fits with the MM83 model gave an acceptable description of the data. Our low  $N_{\text{H}}$  simulation shows that the ASCA SIS is able to detect the discrepancy in the oxygen abundance between the solar and the ISM values. The other abundance differences are not measurable in reasonable amounts of observing time. We note in passing that Ebisawa et al. (1996) indeed found residuals in an observation of the black hole candidate Cygnus X-1 that are very similar to those shown in Fig. 5, which points towards an oxygen abundance of  $\sim 80\%$  solar in the direction to Cyg X-1.

For the large  $N_{\text{H}}$  simulation, the fit to the simulated RXTE PCA spectrum recovered the input parameters for  $\Gamma$  and for  $A_{\text{PL}}$  to two significant digits and found a hydrogen column of  $N_{\text{H}} = 4 \times 10^{22} \text{ cm}^{-2}$ . The residuals shown in Fig. 5 show some structure below 3 keV that is caused by underestimating  $N_{\text{H}}$ , which results in the non-optimal

$\chi^2$  value of the fit ( $\chi_{\text{red}}^2 = 1.7$ ). However, the PCA has significant systematic uncertainties in this region (Wilms et al. 1999), and the deviation seen in our simulation would probably go undetected in a real observational situation.

Although we have not done an exhaustive search of the whole  $N_{\text{H}}$  space, the above result convinces us that for most applications using the current moderate resolution instruments, the models of MM83 and BM92 are sufficient. The physical cause for the underestimate of  $N_{\text{H}}$  is that for energies above 1 keV,  $\sigma_{\text{ISM}}$  is dominated by the metals. Since the abundance ratios of the metals are a result of stellar nucleosynthesis, reducing the metal abundance with respect to hydrogen from the MM83 or BM92 values to our values can be compensated by assuming a different (lower) hydrogen column. Nor does the slightly different shape of  $\sigma_{\text{bf}}$  that results from the updated cross sections produce a noticeable effect in the PCA simulations; the energy resolution of the PCA is insensitive to a difference of this magnitude.

Our simulations for the EPIC pn camera, on the other hand, show deviations on the 5% level when fitted with the MM83 and BM92 models (Fig. 5). These changes are clearly due to the update of the abundances and cross sections. It is for instruments such as the EPIC pn camera that we recommend that our model be used. The EPIC observation simulated here is quite short (the raw EPIC pn count-rate of Cygnus X-1 will be  $\sim 2400$  cps, so that the spectrum used for modeling here has an exposure time of only 4 ksec – shorter than the minimum XMM-Newton observing time of 5 ksec), and the ratio plots in Fig. 5 already show the characteristic curvature due to the deviation in the shape of the cross section assumed in the MM83 models. We note that a similar behavior is also present when fitting the simulated spectrum with the BM92 data. When using the BM92 cross sections, however, it is possible to obtain a good description of the overall absorption by treating the abundances as free parameters. In this case the “wavy” residual structure still remains although the relative abundances found for the elements do come close to the abundances that we assumed in our modeling of  $\sigma_{\text{ISM}}$ . As a result, we recommend using our model whenever high precision work on the 1%–2% level is necessary, as well as in cases when the absorbing column resulting from the spectral fitting process is to be physically interpreted (i.e., when comparing X-ray  $N_{\text{H}}$  values with radio data, or when modeling an observed X-ray spectrum for which the  $N_{\text{H}}$  value is known by other means).

### 3.3. Caveats

While we feel that the model for  $\sigma_{\text{ISM}}$  as presented in the previous sections is well-suited for most X-ray astronomical work, several astronomical or physical issues had to be neglected in the modeling process. In particular, our model does not include the effects of the warm phase or of the ionized phase of the ISM. In addition, we ignore Thomson scattering, which becomes important at moderate to high Thomson optical depths and  $E \gtrsim 4$  keV. These effects have not been included largely because they are negligible for most situations in which our model is likely to be used. Furthermore, the model assumes that there is no variation of the abundances along the line of sight. Finally, we note that energy-dependent scattering by dust grains has

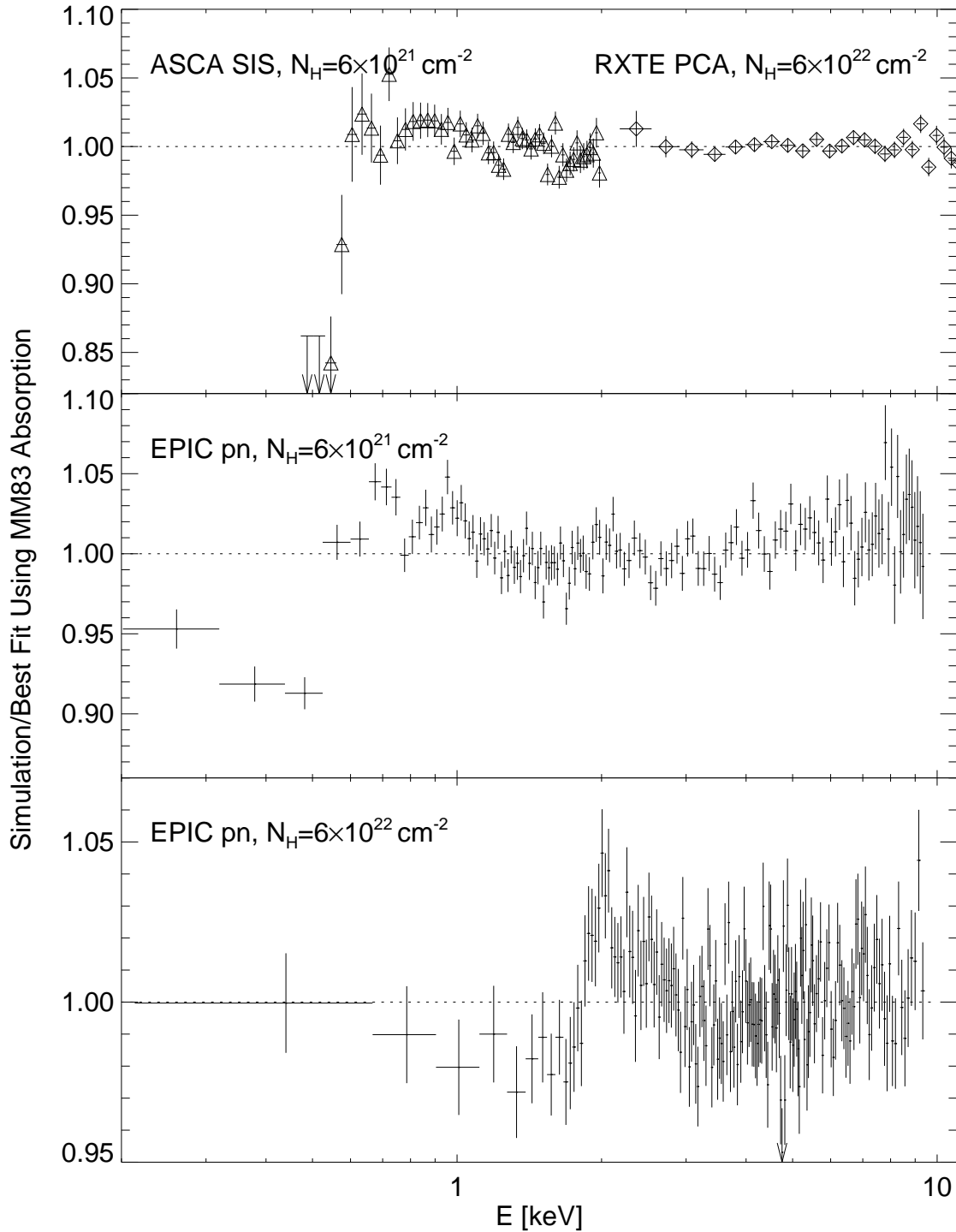


FIG. 5.— Ratio of simulated X-ray data absorbed with our model for  $\sigma_{\text{ISM}}$  to the best fit model using a power-law model and the MM83 models, for the ASCA SIS (triangles), RXTE PCA (diamonds), and the XMM-Newton EPIC pn CCDs. The ASCA SIS simulation with our model is shown for energies below 2 keV. In all cases, the error bars represent Poisson noise. While older models produce adequate fits for the current instruments (with the exception at the O edge, see text), differences of  $\sim 5 \dots 10\%$  are found with the EPIC pn simulations.

not been considered here since an XSPEC routine (`dust`) already exists to treat it.

The warm and ionized phases of the ISM have been neglected here for a number of reasons. Large parts of the ISM are assumed to be (moderately) ionized, and a good model for  $\sigma_{\text{ISM}}$  should in principle include the ionized phase. However, there is even less agreement on the ionization state of the ISM as a whole than there is on the grain phase, which was discussed in §2.4. The major reason for this disagreement is a good one: the ionization of the ISM depends strongly on the line of sight, so that any general model for the ionization structure of the galaxy is prone to fail. It appears, however, that most of the warm phase of the ISM is only moderately ionized, so that our model will still be applicable except for photon energies close to the K-edges. For oxygen, e.g., the K-edge energy increases from 0.54 keV for O I to 0.61 keV for O IV, and the photoionization cross section is also dependent on the ionization stage. It should be noted, though, that the ionization of hydrogen will strongly influence  $\sigma_{\text{ISM}}$  for energies below 0.1 keV. For instance, in their study of soft X-ray emission from other galaxies, (Cui et al. 1996), assumed the ratio between H I and H II to be 1. Using the code presented in Appendix B, this effect may be taken into account by changing the relative abundances of He and the metals with respect to hydrogen.

Similar line of sight effects hold also true for the abundances. In the galaxy, measurement of abundances in HII regions and planetary nebulae has suggested the existence of a radial abundance gradient, particularly at small galactic radii (Rana 1991; Kaufer et al. 1994, and references therein). When computing the absorption of any background object through such a medium with varying abundances, the abundances measured in the X-rays will be the average of the abundance variations along the line of sight. Since the abundances in our model are allowed to vary, it is possible to take this effect into account. Obviously, in such a case the assumed abundance set with respect to which the relative abundances are measured is a matter of taste, and using the solar abundances of Tab. B2 as a baseline instead of the ISM abundances might be a better choice.

Our model also ignores the influence of Thomson scattering because for many observations it will not make a substantial contribution. This is not to say that it is always negligible; Thomson scattering is the dominant physical process for the attenuation of X-rays above  $\sim 10$  keV. As a rough guideline, Thomson scattering should always be included in the modeling process when  $N_{\text{H}} \gtrsim 10^{22} \text{ cm}^{-2}$  (see, e.g., Stelzer et al. 1999). Detailed instructions based on Monte Carlo modeling of Thomson scattering in moderately optically thick media are given by Yaqoob (1997). Note, however, that Yaqoob assumes the electrons to be free. When the electrons are bound, it is more appropriate to consider incoherent scattering, i.e., Compton scattering, off the bound electrons. The cross sections for incoherent scattering and the Klein-Nishina cross section are slightly different (on the percent level), which should be taken into account. Analytical estimates for this effect have been given by Gorshkov, Mikhaïlov & Sherman (1973) for the H atom; for other elements tables are available (Hubbell et al. 1975; Henke, Gullikson & Davis 1993). For most

work, however, these corrections are negligible.

Finally, we also stress that our model, like its predecessors MM83 and BM92, is *not* well suited for extremely high-precision work, e.g., high signal-to-noise spectra with the grating spectrometers on XMM-Newton and *Chandra*. The energy resolution of these very-high-resolution instruments is so high that the X-ray absorption fine structure (XAFS) within grains and molecules might become relevant, as well as resonance effects close to the absorption edges in the absorption cross section itself. For the inclusion of the resonances much higher resolution cross sections than those available here are required. XAFS effects become noticeable especially in regions of large  $N_{\text{H}}$  where grains are an important ingredient. For these studies, dedicated modeling codes are being devised, which should be used instead. See Forrey, Woo & Cho (1998), Woo, Forrey & Cho (1997), Woo (1995), and the references therein, for further details.

### 3.4. Summary and Outlook

We have presented an improved model for the X-ray absorption in the interstellar medium valid above  $\sim 100$  eV by updating the relevant photoionization cross sections and by including the effect of the  $\text{H}_2$  molecule and a revised set of recommended elemental abundances for the interstellar medium. Since the abundances of the metals are smaller than previously estimated, our values of  $\sigma_{\text{ISM}}$  are generally smaller than those used previously. We have shown that these updates will be relevant for instruments to be available as this paper goes into print. We have also reconsidered the effect of grains in the ISM by improving the grain model and the calculation of  $\tau_{\text{grains}}$ , taking into account recent studies of the physical properties of interstellar dust grains. Our results show that the change in opacity due to grains on  $\sigma_{\text{ISM}}$  for realistic grain models and realistic chemical composition of the grains is small. As described in Appendix B, our calculation of  $\sigma_{\text{ISM}}$  is available as a subroutine that can be used with X-ray data analysis packages such as XSPEC.

This work highlights the point made by Shull (1993) and others, that great uncertainties remain in much of the atomic physics data needed to interpret X-ray astronomical observations. The effective areas and energy resolutions of instruments recently launched will be more sensitive than the available atomic data for the X-ray energy range can accommodate, and the situation is even worse for possible future instruments such as Constellation-X or XEUS. The differences between the currently available cross sections discussed in §2.2 are still at the 5% level. We hope that the advent of the new instruments will also initiate new attempts to more accurately determine the atomic data on which X-ray astronomy can rely. We will therefore continue over the next years to update the database of the computations presented here and periodically release new versions of the code presented in Appendix B that will incorporate the improvements in the abundances or the atomic physics.

This work has been partially financed by NASA Grants NGT 5-80, NAG5-7339, and NAG5-7340, and by a National Physical Science Consortium Fellowship grant to AA. JW acknowledges the hospitality of the high energy

astrophysics groups at JILA and at the University of California at San Diego where part of this work was done. We thank the referee Dan McCammon for his comments, which greatly improved the presentation of this paper, and

for providing the code for the helium autoionization resonances. We also thank Laurie Kovalenko, Phil Maloney, Katja Pottschmidt, Richard Rothschild, Rüdiger Staubert, Klaus Werner, and Svet Zhekov for useful comments.

## REFERENCES

- Abramowitz, M., & Stegun, I. A., 1964, Handbook of Mathematical Functions, (Washington: U.S. Government Printing Office), (9th reprint, Mineola: Dover, 1972)
- Allen, C. W., 1960, Astrophysical Quantities, (London: Athlone), 1<sup>st</sup> edition
- Anders, E., & Ebihara, M., 1982, Geochim. Cosmochim. Acta, 46, 2363
- Anders, E., & Grevesse, N., 1989, Geochim. Cosmochim. Acta, 53, 197
- Arabadjis, J. S., & Bregman, J. N., 1999, ApJ, 510, 806
- Arnaud, K. A., 1996, in Astronomical Data Analysis Software and Systems V, ed. J. H. Jacoby, J. Barnes, (San Francisco: Astron. Soc. Pacific), 17
- Bałucińska-Church, M., & McCammon, D., 1992, ApJ, 400, 699
- Band, I. M., Trzhaskovskaya, M. B., Verner, D. A., & Yakovlev, D. G., 1990, A&A, 237, 267
- Bethe, H. A., & Salpeter, E. E., 1957, Quantum Mechanics of One- and Two-Electron Atoms, (Berlin, Göttingen, Heidelberg: Springer)
- Biéumont, E., Baudoux, M., Kurucz, R. L., Ansbacher, W., & Pinnington, E. H., 1991, A&A, 249, 539
- Brinks, E., 1990, in The Interstellar Medium in Galaxies, ed. H. A. Thronson, J. M. Shull, (Dordrecht: Kluwer), 39
- Bronfman, L., Cohen, R. S., Alvarez, H., & Thaddeus, P., 1988, ApJ, 324, 248
- Brown, R. L., & Gould, R. J., 1970, Phys. Rev. D, 1, 2252
- Cardelli, J. A., Meyer, D. M., Jura, M., & Savage, B. D., 1996, ApJ, 467, 334
- Chen, W. F., Cooper, G., & Brion, C. E., 1991, Phys. Rev. A, 44, 186
- Cui, W., Sanders, W. T., McCammon, D., Snowden, S. L., & Womble, D. S., 1996, ApJ, 468, 102
- de Boer, K. S., 1979, ApJ, 229, 132
- de Boer, K. S., 1981, ApJ, 244, 848
- Dove, J. B., Wilms, J., Nowak, M. A., Vaughan, B., & Begelman, M. C., 1998, MNRAS, 289, 729
- Draine, B. T., & Lee, H. M., 1984, ApJ, 285, 89
- Dwek, E., 1997, ApJ, 484, 779
- Ebisawa, K., Ueda, Y., Inoue, H., Tanaka, Y., & White, N. E., 1996, ApJ, 467, 419
- Feldman, U., 1992, Physica Scripta, 46, 202
- Fernley, J. A., Taylor, K. T. & Seaton, M. J., 1987, 20, 6457
- Fireman, E. L., 1974, ApJ, 187, 57
- Fitzpatrick, E. L., 1999, PASP, 111, 63
- Fogel, M. E., & Leung, C. M., 1998, ApJ, 501, 175
- Forrey, R. C., Woo, J. W., & Cho, K., 1998, ApJ, 505, 236
- Gorshkov, V. G., Mikhailov, A. I., & Sherman, S. G., 1973, Sov. Phys. - JETP, 37, 572 (translation of Zh. Ehksp. Teor. Fiz., 64, 1128, 1973)
- Gould, R. J., & Jung, Y.-D., 1991, ApJ, 373, 271
- Grevesse, N., & Anders, E., 1989, in Cosmic abundances of matter, ed. C. Waddington, (New York: AIP Conf. Proc.), 1
- Grevesse, N., & Sauval, A. J., 1999, A&A, 347, 349
- Grevesse, N., Lambert, D. L., Sauval, A. J., van Dishoeck, E. F., Farmer, C. B., & Norton, R. H., 1991, A&A, 242, 488
- Grevesse, N., & Noels, A., 1993, in Origin and Evolution of the Elements, ed. N. Prantzos, E. Vangioni-Flam, M. Casse, (Cambridge: Cambridge Univ. Press), 15
- Gringel, W., et al., 2000, A&A, in preparation
- Henke, B. L., Gullikson, E. M., & Davis, J. C., 1993, Atomic Data Nucl. Data Tables, 54, 181, available at [http://cindy.lbl.gov/optical\\_constants/](http://cindy.lbl.gov/optical_constants/)
- Henke, B. L., Lee, P., Tanaka, T. J., Shimabukuro, R. L., & Fujikawa, B. K., 1982, Atomic Data Nucl. Data Tables, 27, 1
- Hubbell, J. H., et al., 1975, J. Phys. Chem. Ref. Data, 4, 471
- Kaufer, A., et al., 1994, A&A, 289, 740
- Kostik, R., Shchukina, N. G., & Rutten, R. J., 1996, A&A, 305, 325
- Marr, G. V., & West, J. B., 1976, Atomic Data Nucl. Data Tables, 18, 497
- Mathis, J. S., 1990, ARA&A, 28, 37
- Mathis, J. S., 1996, ApJ, 472, 643
- Mathis, J. S., Cohen, D., Finley, J. P., & Krautter, J., 1995, ApJ, 449, 320
- Mathis, J. S., Rumpl, W., & Nordsieck, K. H., 1977, ApJ, 217, 425
- Mathis, J. S., & Whiffen, G., 1989, ApJ, 341, 808
- Meyer, D. M., Cardelli, J. A., & Sofia, U. J., 1997, ApJ, 490, L103
- Meyer, D. M., Jura, M., & Cardelli, J. A., 1998, ApJ, 493, 222
- Morrison, R., & McCammon, D., 1983, ApJ, 270, 119
- Mullman, K. L., Lawler, J. E., Zsargó, J., & Federman, S. R., 1998, ApJ, 500, 1064
- Nicolosi, F., Jannitti, E., & Tondello, G., 1991, J. Physique IV, C1, 89
- O'Donnell, J. E., & Mathis, J. S., 1997, ApJ, 479, 806
- Oza, D. H., 1986, Phys. Rev. A, 33, 824
- Press, W. H., Teukolsky, S. A., Vetterling, W. T., & Flannery, B. P., 1992, Numerical Recipes in FORTRAN, (Cambridge: Cambridge Univ. Press), 2<sup>nd</sup> edition
- Raassen, A. J. J., & Uylings, P. H. M., 1998, A&A, 340, 300
- Rana, N. C., 1991, ARA&A, 29, 129
- Ride, S. K., & Walker, Jr., A. B. C., 1977, A&A, 61, 339
- Samson, J. A. R., & Haddad, G. N., 1994, J. Opt. Soc. Am. B, 11, 277
- Savage, B. D., Bohlin, R. C., Drake, J. F., & Budich, W., 1977, ApJ, 216, 291
- Savage, B. D., & Sembach, K. R., 1996, ARA&A, 34, 279
- Schwalb, M. J., & Predehl, P., 1998, Astron. Nachr., 319, 107
- Shull, J., 1993, Physica Scripta, T47, 165
- Shull, J. M., & Beckwith, S., 1982, ARA&A, 19, 163
- Smith, R. K., & Dwek, E., 1998, ApJ, 503, 831
- Snow, T. P., & Witt, A. N., 1995, Science, 270, 1455
- Snow, T. P., & Witt, A. N., 1996, ApJ, 468, L65
- Sofia, U. J., Cardelli, J. A., & Savage, B. D., 1994, ApJ, 430, 650
- Stelzer, B., Wilms, J., Staubert, R., Gruber, D., & Rothschild, R., 1999, A&A, 342, 736
- Strom, S. E., & Strom, K. M., 1961, PASP, 73, 43
- Verner, D. A., & Yakovlev, D. G., 1995, A&AS, 109, 125
- Verner, D. A., Yakovlev, D. G., Band, I. M., & Trzhaskovskaya, M. B., 1993, Atomic Data Nucl. Data Tables, 55, 233
- Wilms, J., Nowak, M. A., Dove, J. B., Fender, R. P., & di Matteo, T., 1999, ApJ, in press
- Wolff, M. J., Clayton, G. C., & Gibson, S. J., 1998, ApJ, 503, 815
- Woo, J. W., 1995, ApJ, 447, L129
- Woo, J. W., Clark, G. W., Day, C. S. R., Nagase, F., & Takeshima, T., 1994, ApJ, 436, L5
- Woo, J. W., Forrey, R. C., & Cho, K., 1997, ApJ, 477, 235
- Wright, E. L., 1987, ApJ, 320, 818
- Yan, M., Sadeghpour, H. R., & Dalgarno, A., 1998, ApJ, 496, 1044
- Yaqoob, T., 1997, ApJ, 479, 184

## APPENDIX

## SELF-SHIELDING IN THE GRAINS

To derive the optical depth of the grains (eq. [5]) we consider a population of grains of homogeneous chemical composition with size  $a$ , geometrical cross section  $\sigma_{\text{geom}}$ , column density  $\langle N \rangle$ , and average photoionization cross section  $\langle \sigma \rangle$  (per atom). For grains of realistic shape,  $\langle N \rangle$  is a complicated function of  $a$ . Since the influence of grains on  $\sigma_{\text{ISM}}$  is small, however, for simplicity we can assume that the grains are spheres with radius  $a$  so that

$$\langle N \rangle = \frac{4\rho a}{3\mu} = \frac{4na}{3} \quad (\text{A1})$$

where  $\rho$  is the mass density of the grain,  $n$  the number density of the grain, and  $\mu$  the mean molecular weight of the grains constituents. Using the notation of Section 2.1,  $\mu$  is given by

$$\mu = \frac{\sum_Z A_Z \cdot \beta_Z \cdot \mu_Z}{\sum_Z A_Z \cdot \beta_Z} \quad (\text{A2})$$

Here,  $\mu_Z$  is the molecular weight of element  $Z$  (Tab. B2). For the default abundances and depletions of Tab. B2,  $\mu = 18.2 \text{ amu} = 3.0 \times 10^{-23} \text{ g/atom}$ . Assuming  $\rho = 1 \text{ g cm}^{-3}$ , the grain number density is  $n = 3.3 \times 10^{22} \text{ atoms cm}^{-3}$ . Ignoring solid state effects, the photoionization cross section of the grain material is given by

$$\langle \sigma \rangle = \frac{\sum_Z A_Z \cdot \beta_Z \cdot \sigma_{\text{bf}}(Z)}{\sum_Z A_Z \cdot \beta_Z} \quad (\text{A3})$$

For a column density  $N_{\text{grains}}$  of grains of a *single size* along the line of sight, the optical depth for photoabsorption of the grains is the product between the geometrical optical depth of the grains,  $N_{\text{grains}}\sigma_{\text{geom}}$ , and the fraction of photons that encounter the grain and are absorbed:

$$\tau_{\text{grains}} = N_{\text{grains}}\sigma_{\text{geom}} (1 - \exp(-\langle \sigma \rangle \langle N \rangle)). \quad (\text{A4})$$

In computing  $\sigma_{\text{ISM}}$  for grains of a single size it is sometimes convenient to express  $\tau_{\text{grains}}$  in terms of the optical depth that would be observed if the constituents of the grain were in the gaseous phase,  $\tau_{\text{grains}} = f N_{\text{gas}} \langle \sigma \rangle$ . Hence,

$$f = \frac{N_{\text{grains}}\sigma_{\text{geom}}}{N_{\text{gas}}\langle \sigma \rangle} (1 - \exp(-\langle \sigma \rangle \langle N \rangle)) = \frac{1 - \exp(-\langle \sigma \rangle \langle N \rangle)}{\langle \sigma \rangle \langle N \rangle}. \quad (\text{A5})$$

since the column density of the grain is  $N_{\text{gas}}/(N_{\text{grains}}\sigma_{\text{geom}})$ . This factor is called the self-blanketing factor (Fireman 1974).

For the general case that the grains have a *size distribution*  $dn_{\text{gr}}(a)/da$ , where

$$\int_0^\infty \frac{dn_{\text{gr}}}{da} da = 1 \quad (\text{A6})$$

a similar derivation shows that

$$\tau_{\text{grains}} = N_{\text{H}}\xi_{\text{g}} \int_0^\infty \frac{dn_{\text{gr}}(a)}{da} \sigma_{\text{geom}} (1 - \exp(-\langle \sigma \rangle \langle N \rangle)) da, \quad (\text{A7})$$

where  $\xi_{\text{g}}$  is the number of grains per hydrogen atom along the line of sight. For spherical grains,

$$\xi_{\text{g}} = \frac{\sum_Z A_Z \cdot \beta_Z \cdot \mu_Z}{\int \frac{dn_{\text{gr}}}{da} \cdot \rho \cdot \frac{4}{3}\pi a^3 \cdot da} \quad (\text{A8})$$

For a power-law size distribution,  $dn_{\text{gr}}(a)/da = ka^{-p}$ , where  $a_{\text{min}} \leq a \leq a_{\text{max}}$ , we can express  $\tau_{\text{grains}}$  in terms of special functions. Inserting  $\sigma_{\text{geom}} = \pi a^2$  into equation (A7) and performing a partial integration, we obtain for  $p < 4$

$$\begin{aligned} \tau_{\text{grains}} = N_{\text{H}}\xi_{\text{g}} \frac{\pi k}{p-3} \left\{ \frac{1}{a_{\text{min}}^{p-3}} \left( 1 - e^{-4\langle \sigma \rangle n a_{\text{min}}/3} \right) - \frac{1}{a_{\text{max}}^{p-3}} \left( 1 - e^{-4\langle \sigma \rangle n a_{\text{max}}/3} \right) \right. \\ \left. + (4\langle \sigma \rangle n/3)^{p-3} [\gamma(4-p, 4\langle \sigma \rangle n a_{\text{max}}/3) - \gamma(4-p, 4\langle \sigma \rangle n a_{\text{min}}/3)] \right\}, \end{aligned} \quad (\text{A9})$$

where the incomplete gamma function is given by (Abramowitz & Stegun 1964, section 6.5)

$$\gamma(\alpha, x) = \int_0^x e^{-t} t^{\alpha-1} dt \quad (\text{A10})$$

and can be evaluated using algorithms presented by Press et al. (1992, Section 6.2).

#### IMPLEMENTATION INTO XSPEC

Using the formalism and data described in Section 2, we have written subroutines that can be used in conjunction with the popular X-ray data analysis package XSPEC (Arnaud 1996). These subroutines are available at:

<http://astro.uni-tuebingen.de/nh/>

Given the uncertainty of many of the parameters entering the model, there are several interfaces to the subroutine. The main spectral model, `tbabs`, is intended as a replacement for the earlier `wabs` and `phabs` models, as well as their redshifted versions. This model assumes the abundances and depletion factors of Table B2. A subroutine `ztbabs` for modeling redshifted absorption is also available. The latter subroutine does not account for the dust component, as X-ray observations with a measurable dust influence will most probably only include observations of galactic objects, at least within the next decade.

In addition, the XSPEC model `tbvarabs` provides a full interface to the X-ray absorption model presented in Section 2 and allows the user to change all abundances, depletion factors, and grain properties. We stress that this model is very powerful and therefore prone to misuse. Caution is required when fitting data with too many free parameters.

TABLE B1  
FIT COEFFICIENTS  $a_i$  TO EQUATION (6) FOR THE H<sub>2</sub> PHOTOABSORPTION CROSS SECTION.

$a_0$	$a_1$	$a_2$	$a_3$	$a_4$	$a_5$
0.664	-11.768	78.118	-231.339	368.053	-189.953

TABLE B2  
MOLECULAR WEIGHT, K EDGE ENERGIES, ABUNDANCES AND DEPLETION FACTORS  $1 - \beta_Z$  FOR THE ABUNDANT ELEMENTS.

Element	$\mu_Z^a$	$E_K^b$ keV	$12 + \log A_Z$		$1 - \beta_Z^e$			
			solar <sup>c</sup>	ISM <sup>d</sup>	this paper	MM83 <sup>f</sup>	Ride77 <sup>g</sup>	
1	H	1	...	12.00	12.00	1.0	1.0	1.0
2	He	4	...	10.99	10.99	1.0	1.0	1.0
6	C	12	0.29	8.60	8.38	0.5	0.0	0.2
7	N	14	0.41	7.97	7.88	1.0	0.0	0.5
8	O	16	0.54	8.93	8.69	0.6	0.75	0.5
10	Ne	20	0.87	8.09	7.94	1.0	1.0	1.0
11	Na	23	1.08	6.31	6.16	0.25	0.0	...
12	Mg	24	1.31	7.59	7.40	0.2	0.0	0.2
13	Al	27	1.57	6.48	6.33	0.02	0.0	...
14	Si	28	1.85	7.55	7.27	0.1	0.0	0.5
15	P	31	2.15	5.57	5.42	0.6	...	...
16	S	32	2.48	7.27	7.09	0.6	0.0	0.7
17	Cl	35	2.83	5.27	5.12	0.5	0.0	...
18	Ar	40	3.20	6.56	6.41	1.0	1.0	0.5
20	Ca	40	4.04	6.34	6.20	0.003	0.0	...
22	Ti	48	4.97	4.93	4.81	0.002	...	...
24	Cr	52	5.97	5.68	5.51	0.03	0.0	...
25	Mn	55	6.55	5.53	5.34	0.07	...	...
26	Fe	56	7.12	7.50	7.43	0.3	0.0	0.2
27	Co	59	7.73	4.92	4.92	0.05	...	...
28	Ni	59	8.35	6.25	6.05	0.04	0.0	...

<sup>a</sup>molecular weight in amu,

<sup>b</sup>K edge energy (rounded after Verner & Yakovlev 1995)

<sup>c</sup>solar abundance (Anders & Grevesse 1989; Grevesse et al. 1991; Grevesse & Noels 1993, see also §2.3),

<sup>d</sup>adopted abundance of the ISM based on Snow & Witt (1996), Cardelli et al. (1996), Meyer, Cardelli & Sofia (1997) and Meyer, Jura & Cardelli (1998), see §2.3;

<sup>e</sup>ratio of gas abundance to total ISM abundance,  $1 - \beta_Z$ , using our adopted abundances (§2.4). For comparison, the older values of

<sup>f</sup>Morrison & McCammon (1983), and

<sup>g</sup>Ride & Walker (1977) are also listed.